JOURNAL OF GEOPHYSICAL RESEARCH, VOL. 112, D21102, doi:10.1029/2007JD008428, 2007

An RM-NN algorithm for retrieving land surface temperature and emissivity from EOS/MODIS data

Kebiao Mao,[1,2,3] Jiancheng Shi,[4,5] Zhao-Liang Li,[6,7] and Huajun Tang[8]

Received 18 January 2007; revised 27 April 2007; accepted 28 June 2007; published 1 November 2007.

[1] Three radiative transfer equations are built for MODIS bands 29, 31, and 32, which involve six unknown parameters (average atmospheric temperature, land surface temperature (LST), three band emissivities, and water vapor content). The relationships between geophysical parameters have been analyzed in detail, which indicates that neural network is one of the best methods to resolve these ill-posed problems (LST and emissivity). Retrieval analysis indicates that the combined radiative transfer model (RM) with neural network (NN) algorithm can be used to simultaneously retrieve land surface temperature and emissivity from Moderate-Resolution Imaging Spectroradiometer (MODIS) data. Simulation data analysis indicates that the average error of LST is under 0.4 K and the average error of emissivity is under 0.008, 0.006, and 0.006 for bands 29, 31, and 32, respectively. The comparison analysis between retrieval result by RM-NN and MODIS product algorithm indicates that the generalized split window LST overestimates the emissivity and underestimates land surface temperature. The retrieval results by RM-NN lie between the two products provided by NASA and closer to day/night LST algorithm after statistics analysis. The average error is 0.36 K relative to MODIS LST product (MOD11_L2) retrieved by generalized split window algorithm if we make a regression revision. The comparison of retrieval results with ground measurement data in Xiaotangshan also indicates that the RM-NN can be used to retrieve accurately land surface temperature and emissivity.

Citation: Mao, K., J. Shi, Z.-L. Li, and H. Tang (2007), An RM-NN algorithm for retrieving land surface temperature and emissivity from EOS/MODIS data, *J. Geophys. Res.*, *112*, D21102, doi:10.1029/2007JD008428.

1. Introduction

[2] The extensive requirement of temperature information at a large scale for environmental studies and management activities of the Earth's sources has made the remote sensing of land surface temperature (LST) and emissivity an important issue in recent decades. Many efforts have been devoted to the establishment of methodology for retrieving LST and emissivity from remote sensing data.

[3] Many split window methods have been developed to retrieve land surface temperature from NOAA/AVHRR and Moderate-Resolution Imaging Spectroradiometer (MODIS) data. The split window method utilizes the differential absorption in adjacent thermal bands to correct the atmospheric effects [*Price*, 1984; *Becker and Li*, 1990; *Sobrino and Caselles*, 1991; *Sobrino et al.*, 1994; *Coll et al.*, 1994; *Vidal*, 1991; *Kerr et al.*, 1992; *Otlle and Stoll*, 1993; *Prata*, 1994; *Wan and Dozier*, 1996; *Qin et al.*, 2001a, 2001b; *Sobrino et al.*, 2004; *Mao et al.*, 2005a, 2005b, 2005c]. The form of these algorithms is the same as the general one, but the calculation of parameters is different. The accuracy of most algorithms is very high, but they still need make some assumptions and some prior knowledge of emissivity and atmosphere (especially water vapor content).

[4] It is very difficult to retrieve simultaneously land surface temperature and emissivity from thermal radiance measurements, because a single multispectral thermal measurement with N bands corresponds to N equations in N + 1 unknowns (N spectral emissivities and LST), which is a typical ill-posed inversion problem. Without any prior information, it is almost impossible for us to accurately

[1]Permanently at Key Laboratory of Resources Remote Sensing and Digital Agriculture, Ministry of Agriculture, Hulumber Grassland Ecosystem Observation and Research Station, Institute of Agricultural Resources and Regional Planning, Ministry of Agriculture, Chinese Academy of Agricultural Sciences, Beijing, China.
[2]Formerly at State Key Laboratory of Remote Sensing Science, Beijing, China.
[3]Temporarily at Graduate School of Chinese Academy of Sciences, Beijing, China.
[4]Visiting professor from State Key Laboratory of Remote Sensing Science, Beijing, China.
[5]Permanently at Institute for Computational Earth System Science, University of California, Santa Barbara, California, USA.
[6]Institute of Geographic Sciences and Natural Resources Research, Chinese Academy of Sciences, Beijing, China.
[7]Visiting professor from Laboratoire des Sciences de l'Image, de l'Informatique et da la Télédétection/Ecole Nationale Superieure de Physique de Strasbourg, UMR 7005, Ilkirch, France.
[8]Key Laboratory of Resources Remote Sensing and Digital Agriculture, Ministry of Agriculture, Hulumber Grassland Ecosystem Observation and Research Station, Institute of Agricultural Resources and Regional Planning, Ministry of Agriculture, Chinese Academy of Agricultural Sciences, Beijing, China.

0148-0227/07/2007JD008428$09.00

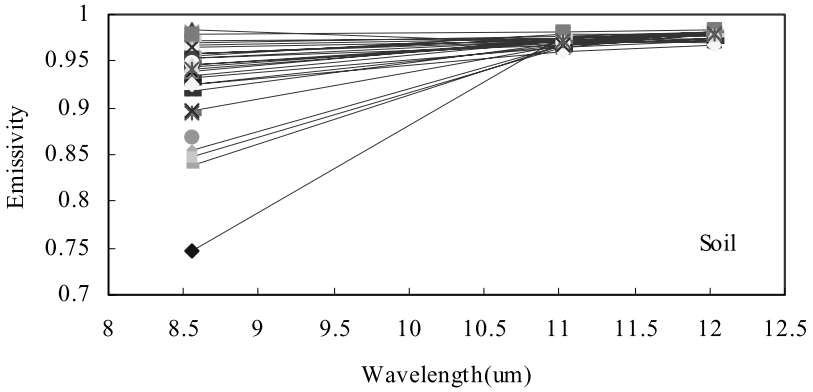

Figure 1a. The soil emissivity in three thermal bands of MODIS data.

retrieve both LST and emissivity. *Kahle and Alley* [1992], *Hook et al.* [1992], *Watson* [1992], *Kealy and Hook* [1993], *Schmugge et al.* [1998, 2002], *Liang* [2001], and *Mao et al.* [2005a, 2005b, 2005c, 2006] made a lot of researches for the separation of land surface temperature and emissivity. *Li and Becker* [1993] proposed a method to estimate both land surface emissivity and LST using pairs of day/night coregistered AVHRR images, which needs atmosphere profile information. This algorithm assumes that the emissivity is the same at day and nighttime. *Gillespie et al.* [1998] proposed an algorithm to separate emissivity and land surface temperature for high-resolution thermal image ASTER, and its accuracy is mainly determined by atmosphere correction.

[5] MODIS is 36 bands EOS instrument, which is particularly useful because of its global coverage, radiometric resolution and dynamic ranges, and accurate calibration in multiple thermal infrared bands designed for retrievals of SST, LST and atmospheric properties [*Salomonson et al.*, 1989; *King et al.*, 1992]. *Wan and Dozier* [1996] proposed a generalized split window algorithm for retrieving land surface temperature from MODIS, and the emissivity is obtained from classification information. The generalized split window algorithm in most cases, has been validated within ±1 K in clear-sky conditions, with in situ measurement data collected in field campaigns over lakes, silt playa, grasslands and agricultural fields [*Wan et al.*, 2002, 2004; *Coll et al.*, 2005]. *Wan and Li* [1997] proposed a day/night algorithm to retrieve LST and land surface emissivity from MODIS, which needs day and night image data and assumes that the emissivity is not changed at the same location. For example, if there is big rainfall in day but it is clear in night, the accuracy cannot be guaranteed because the emissivity has changed.

[6] In this paper, we will present why and how to use a combined radiative transfer model (RM)–neural network (NN) algorithm to retrieve land surface temperature and emissivity from MODIS1B data. In section 2, the ill-posed problem of land surface temperature and emissivity has been discussed. In section 3, the interconnections between geophysical parameters are analyzed in detail by using spectral database provided by Jet Propulsion Laboratory (JPL: URL http://speclib.jpl.nasa.gov) and simulation data by using MODTRAN4 [*Berk et al.*, 2003], which indicate that the ill-posed retrieval problem can be overcome if we can make full use of the relationships between geophysical parameters. In section 4, the neural network is considered as one of the best methods for resolving the retrieval problem (LST and emissivity) because it owns function approximation, optimization computation and classification ability. To some extent, the neural network can overcome some shortcomings of previous algorithms, which does not require the derivation of rules and combines some classification information. The neural network determines the inverse mappings and functional relation directly from a radiative transfer model (RM). RM-NN algorithm can eliminate the

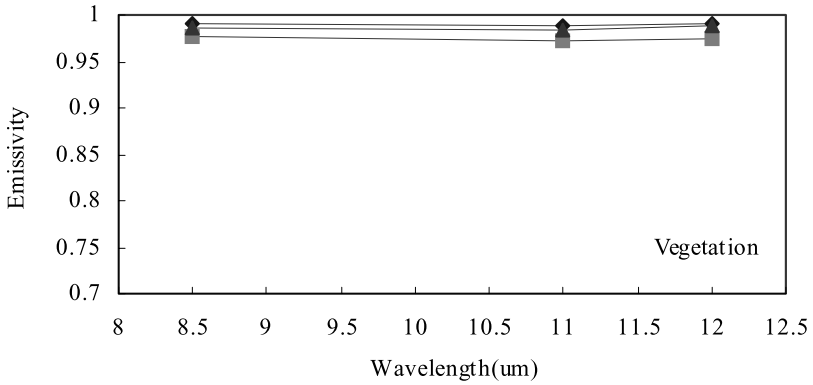

Figure 1b. The vegetation emissivity in three thermal bands of MODIS data.

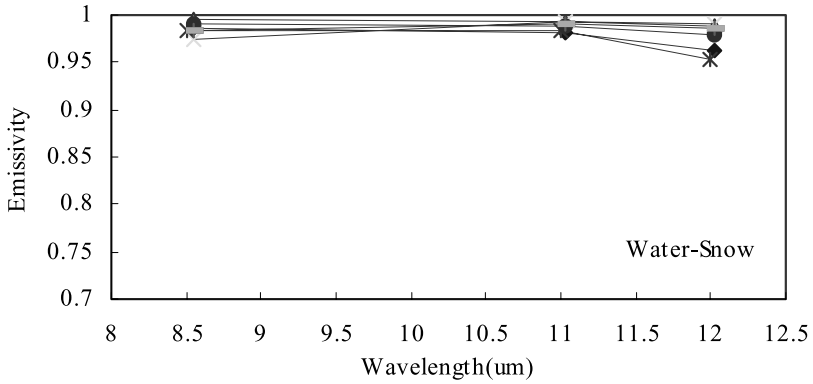

Figure 1c. The water-snow emissivity in three thermal bands of MODIS data.

need for the development of an algorithmic procedure and a set of rules undertaking that, in general, has been found to be costly and time consuming (section 3). In section 5, the comparison evaluation will be made between the retrieval results by RM-NN and MODIS LST product.

2. Posed Problem of Land Surface Temperature and Emissivity Retrieved From MODIS Data

[7] The land surface temperature and emissivity retrieval are based on the thermal radiance of the ground and its transfer from the ground through the atmosphere to the remote sensor. Generally speaking, the ground is not a blackbody. Thus ground emissivity has to be considered for computing the thermal radiance emitted by the ground. Atmosphere has important effects on the received radiance at remote sensor level. Considering all these impacts, the general radiance transfer equation [*Otlle and Stoll*, 1993] for remote sensing of LST can be formulated as follows:

$$B_i(T_i) = \tau_i(\theta)\left[\varepsilon_i(\theta)B_i(T_s) + (1-\varepsilon_i(\theta))I_i^{\downarrow}\right] + I_i^{\uparrow} \tag{1}$$

where T_s is the LST, T_i is the brightness temperature in channel i at satellite, $\tau_i(\theta)$ is the atmospheric transmittance in channel i at viewing direction θ(zenith angle from nadir), and $\varepsilon_i(\theta)$ is the ground emissivity in channel i at viewing direction θ. $B_i(T_s)$ is the ground radiance, $I_i^{\uparrow}$ and $I_i^{\downarrow}$ are the upwelling and downwelling atmospheric radiances, respectively. $I_i^{\uparrow}$ and $I_i^{\downarrow}$, can be depicted as

$$I_i^{\uparrow} = (1-\tau_i(\theta))B_i(T_a) \tag{2a}$$

$$I_i^{\downarrow} = (1-\tau_i(\theta'))B_i\left(T_a^{\downarrow}\right) \tag{2b}$$

Where T_a is the effective average temperature of upward radiance of atmosphere. $T_a^{\downarrow}$ is effective average temperature of downward radiance of atmosphere. θ' is the downwelling direction of atmospheric radiance. The detailed derivation can be referred to *França and Cracknell* [1994] and *Qin et al.* [2001a, 2001b]. Substituting (2) to (1), we have

$$B_i(T_i) = \varepsilon_i(\theta)\tau_i(\theta)B_i(T_s) + [1-\tau_i(\theta)][1-\varepsilon_i(\theta)]\tau_i(\theta) B_i\left(T_a^{\downarrow}\right) + [1-\tau_i(\theta)]B_i(T_a) \tag{3}$$

Qin et al. [2001a, 2001b] made some reasonable simplification and some analysis. They got a conclusion that it has not much influence if we use T_a instead of $T_a^{\downarrow}$, so the equation can be depicted as equation (4).

$$B_i(T_i) = \varepsilon_i(\theta)\tau_i(\theta)B_i(T_s) + [1-\tau_i(\theta')][1-\varepsilon_i(\theta)]\tau_i(\theta) B_i(T_a) + [1-\tau_i(\theta)]B_i(T_a) \tag{4}$$

[8] In equation (4), there are three unknowns (one band emissivity, land surface temperature, effective average

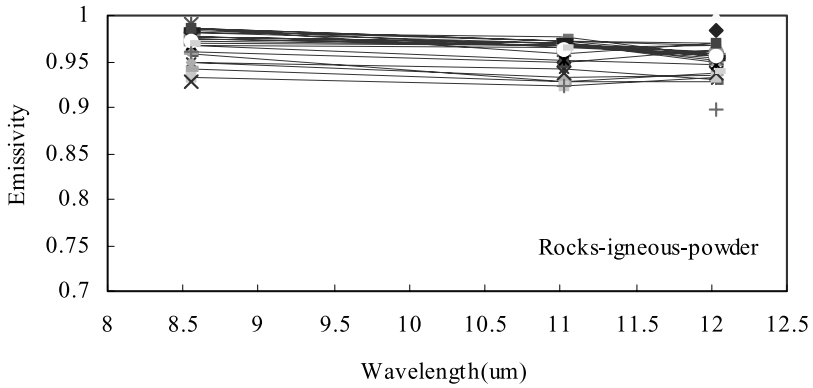

Figure 1d. The rock-igneous powder emissivity in three thermal bands of MODIS data.

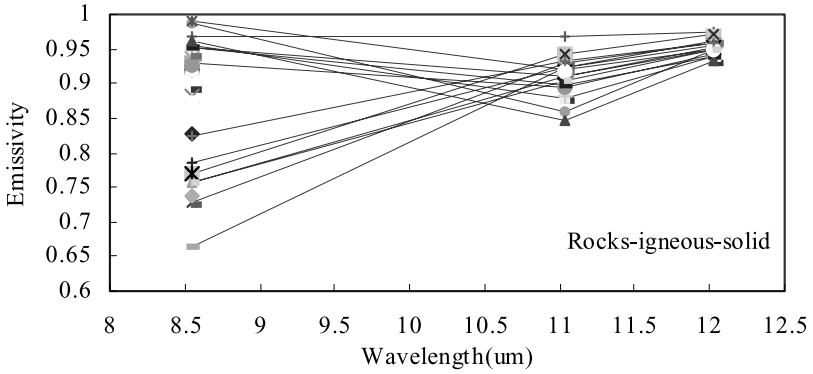

Figure 1e. The rocks-igneous-solid emissivity in three thermal bands of MODIS data.

atmospheric temperature) in one equation. On the other hand, the individual band transmittance (τ) is also an unknown when the atmospheric column water vapor cannot be obtained. So we cannot resolve the equations and must find other condition, which is a typical ill-posed retrieval problem.

[9] According to the MODIS band specification by *Salomonson et al.* [1989] and *Wan and Li* [1997], bands 20, 22, and 23 are in the transparent atmospheric window in the 3.5–4.2 μm medium wavelength range which is influenced by sun radiance in daytime, while bands 29–32 are in the 8–13 μm atmospheric window range which is influenced little by sun radiance. Band 30 is strongly affected by ozone absorption, so bands 29, 31, and 32 (8.4–8.7, 10.78–11.28, and 11.77–12.27 μm) are most suitable for retrieving land surface temperature from MODIS data. The radiative transfer equations for MODIS bands 29, 31, and 32 can be written as

$$B_{29}(T_{29}) = \varepsilon_{29}(\theta)\tau_{29}(\theta)B_{29}(T_s) + [1-\tau_{29}(\theta')][1-\varepsilon_{29}(\theta)]\tau_{29}(\theta) B_{29}(T_a) + [1-\tau_{29}(\theta)]B_{29}(T_a) \quad (5a)$$

$$B_{31}(T_{31}) = \varepsilon_{31}(\theta)\tau_{31}(\theta)B_{31}(T_s) + [1-\tau_{31}(\theta')][1-\varepsilon_{31}(\theta)]\tau_{31}(\theta) B_{31}(T_a) + [1-\tau_{31}(\theta)]B_{31}(T_a) \quad (5b)$$

$$B_{32}(T_{32}) = \varepsilon_{32}(\theta)\tau_{32}(\theta)B_{32}(T_s) + [1-\tau_{32}(\theta')][1-\varepsilon_{32}(\theta)]\tau_{32}(\theta) B_{32}(T_a) + [1-\tau_{32}(\theta)]B_{32}(T_a) \quad (5c)$$

[10] In equations (5a)–(5c), there are six unknowns (three band emissivities, land surface temperature, effective average atmospheric temperature and water vapor content (transmittance)) in three equations, so we cannot resolve the equations and must find other condition. The effective average atmospheric temperature (T_a) is defined by *Sobrino and Caselles* [1991].

$$T_a = \frac{1}{w}\int_0^Z T_z\, dw(z, Z) \quad (6)$$

where w is the total water vapor content of atmosphere from 0 to Z, $dw(z, Z)$is water vapor content in atmosphere at height z, T_z is the atmosphere temperature in height z. In fact, the effective average atmosphere temperature (T_a) varies with the wavelength dependence of the water vapor absorption. The influence is slight, especially when we use iterative method (such as neural network) to resolve retrieval equations. Here, we just make effective average atmosphere temperature as one unknown.

3. Interconnection of Geophysical Parameters

[11] The geophysical parameters are not independent with each other. We did not make fully use of the interconnection between them in the previous algorithms. In this section, we will explore the relationships between different band emissivities in MODIS bands 29, 31, and 32 about 160 kinds of surface types provided by JPL (URL http://speclib.jpl.nasa.gov), between land surface temperature, brightness temperature at satellite, and effective average atmosphere temperature, and also between transmittance and water vapor content.

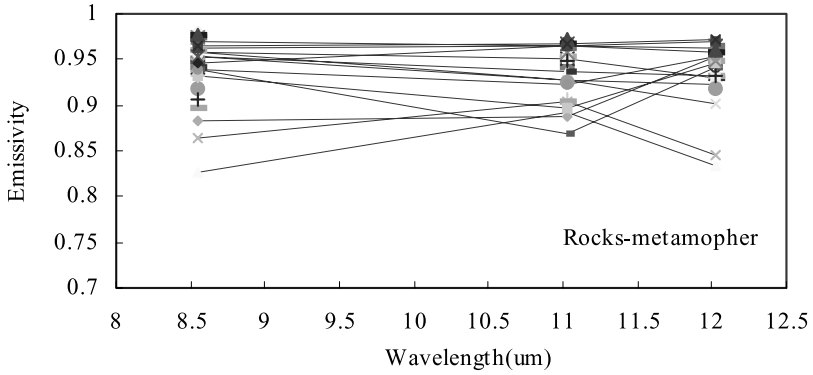

Figure 1f. The rocks-metamopher emissivity in three thermal bands of MODIS data.

Table 1. Local Linear Approximate Error for the Emissivity of Band 32[a]

Type	Average Error	RMS	Range
Soil	0.0027	0.008	0.0001∼0.0088
Vegetation	0.0015	0.002	0.0007∼0.0022
Water-snow	0.003	0.004	0.0002∼0.0053
Rocks-igneous powder	0.0036	0.0046	0.0002∼0.008
Rocks-igneous-solid	0.0071	0.0106	0.0001∼0.0076
Rocks-metamopher	0.018	0.0242	0.001∼0.0586

[a]For rock-igneous powder the one is larger than 0.014; for rocks-igneous-solid five are larger than 0.01.

3.1. Connection of Emissivity Between Bands

[12] As we all know that the split window algorithm assumes the emissivity as a known parameter. The main reason is that the number of equations is less than unknowns and the emissivity is almost a constant for every surface type in the range of thermal band. The emissivity is mainly determined by the structure of the ground surface and range of band, and changed with the wavelength. We analyze the emissivity of common terrestrial materials about 160 kinds provided by JPL (URL http://speclib.jpl.nasa.gov). The emissivity ($\varepsilon_i(\theta)$) depends on emission angle θ [*Dozier and Warren*, 1982]. The spectral emissivity database provided by JPL does not contain information about emission angles. It is very difficult to obtain the angle information, so we assume that the emissivity is same at all orientation in database. Because the curve of emissivity is continuity and stable, we can utilize a local linear equation to describe approximately the change of emissivity in a short range of wavelength. The emissivity of most terrestrial materials is higher than 0.65 and changes very slight in the ranges of MODIS bands 29–33 (8.5 $\sim$ 13 μm). Especially for bands 31 and 32, the wavelength of band is very short and almost continuity. Under 1 km scale of MODIS data, the land surface is mainly made up of four types (soil, vegetation, water and rock). We will make a detailed analysis as following. For the first type soil, the spectral database provides about 41 kinds (like Figure 1a). As shown in Figure 1a, the difference of emissivity for bands 31 and 32 is very small, and the trend is almost same. However, the emissivity of band 29 is very different from bands 31 and 32. We make regression for emissivity of 41 types of soil and obtain expression (7a). For the second type vegetation, the spectral database just provides four typical types (Figure 1b) because the curve is almost same for different vegetation. We make a regression for emissivity of four types of vegetation and obtain expression (7b). For the third type snow-water, the spectral database provides about nine typical types and the curve is almost same for different types (like Figure 1c). We make regression for emissivity of nine snow-water types and obtain expression (7c). It should also be noted that the JPL spectral database uses the measurements from Johns Hopkins for spectral emissivity of snow. In the literature there is a conflict between these measurements and interpretations and those of others [*Dozier and Painter*, 2004]. The JHU data show decreasing emissivity as the grains get larger, whereas scattering theory would lead to the opposite conclusion, which need us to modify and compensate more spectral curve in future.

$$\varepsilon_{32} = 0.5813 + 0.4082\varepsilon_{31} \tag{7a}$$

$$\varepsilon_{32} = -0.124 + 1.129\varepsilon_{31} \tag{7b}$$

$$\varepsilon_{32} = -2.1105 + 3.1226\varepsilon_{31} \tag{7c}$$

[13] The spectral curve of rocks is very different relative to the previous three main types above. JHU, JPL, and USGS classify them into three classes (powder, solid and metamopher) and the detailed introduction can be referred to (URL http://speclib.jpl.nasa.gov). The first is rock-igneous powder and the spectral data provides about 35 types (like Figure 1d). We make regression for emissivity of 35 rock-igneous powder types and obtain expression (7d). The second one is rock-igneous solid and the spectral data provides about 35 types (like Figure 1e). We make regression for emissivity of 35 rock-igneous solid types and obtain expression (7e). The third one is rocks-metamopher

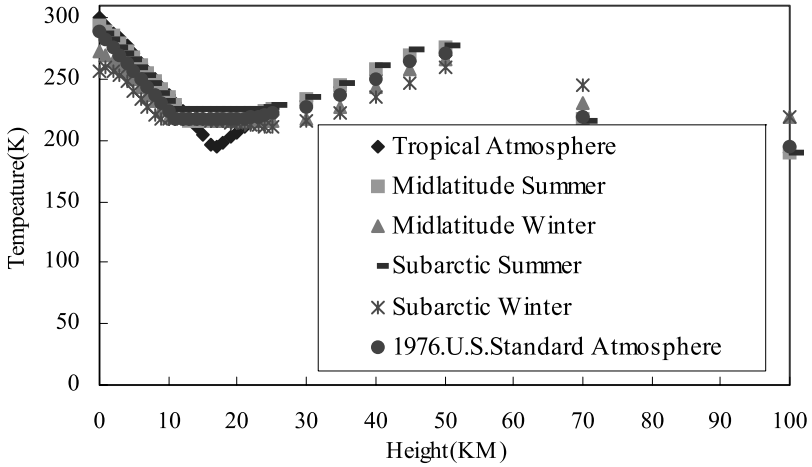

Figure 2. Six standard atmosphere temperature profiles.

Table 2. Ratio of Water Vapor Content to the Total in Different Atmospheric Profiles

Altitude, km	Tropical Atmosphere	Midlatitude Summer	Midlatitude Winter	Subarctic Summer	Subarctic Winter	USA 1976
0	0.369	0.38	0.337	0.354	0.249	0.341
1	0.253	0.253	0.241	0.234	0.249	0.243
2	0.181	0.16	0.174	0.164	0.196	0.167
3	0.0913	0.0895	0.116	0.105	0.141	0.104
4	0.0427	0.0515	0.0636	0.0661	0.0851	0.0637
5	0.0291	0.0271	0.0366	0.0389	0.0416	0.037
6	0.0166	0.0166	0.0202	0.021	0.0204	0.022
7	0.00913	0.01	0.00822	0.0113	0.0112	0.0121
8	0.00486	0.0057	0.00337	0.00508	0.00229	0.00693
9	0.00233	0.00325	0.00154	0.00147	0.00174	0.00266
10	0.000972	0.00174	0.000722	0.000426	0.001	0.00104
11	0.00033	0.000596	0.000209	0.000115	0.000428	0.000474
12	0.000116	0.000163	0.000108	0.0000445	0.000219	0.000214
13	0.000035	0.0000391	0.0000771	0.0000284	0.000139	0.000104
14	0.0000194	0.0000209	0.0000634	0.0000219	0.00012	0.0000484
15	0.0000109	0.0000121	0.0000533	0.0000189	0.000104	0.000035

and the spectral data provides about 23 types (like Figure 1f). We make regression for emissivity of 23 rocks-metamopher types and obtain expression (7f). The linear relationship is worst than before. The detailed information of approximate error of band 32 can be referenced with Table 1.

$$\varepsilon_{32} = 0.6177 + 0.3678\varepsilon_{31} \tag{7d}$$

$$\varepsilon_{32} = 0.2959 + 0.6844\varepsilon_{31} \tag{7e}$$

$$\varepsilon_{32} = -0.2367 + 1.2461\varepsilon_{31} \tag{7f}$$

[14] We analyzed JPL's emissivity data on 80 kinds of the most common terrestrial materials [*Wan and Li*, 1997] (URL http://speclib.jpl.nasa.gov). After some analysis for the curve of emissivity, the land surface can be simply classified into two groups. The first is land surface covered by none-water/snow, and the relationship between band emissivities can be written using equations (7a)–(7f).

$$\varepsilon_{31} = 0.0749 + 0.057\varepsilon_{29} + 0.862\varepsilon_{32} \tag{8}$$

The second is land surface covered by water and snow, and the relationship between band emissivities can be written as equation (8):

$$\varepsilon_{31} = 0.6836 + 0.0357\varepsilon_{29} + 0.2763\varepsilon_{32} \tag{9}$$

For none-water/snow covered surface, the average emissivity error of band 31 is under 0.0031. For water and snow covered surface, the average emissivity error of band 32 is under 0.0011.

[15] Although surface types is very complex (like man-made terra), the land surface is mainly made up of four types (soil, vegetation, water, rocks) under 1 km scale of MODIS data. In fact, as shown in spectral curve above, we can make classification through thermal band because difference and interconnection are contained within them. We can get more equations to describe them and the ill-

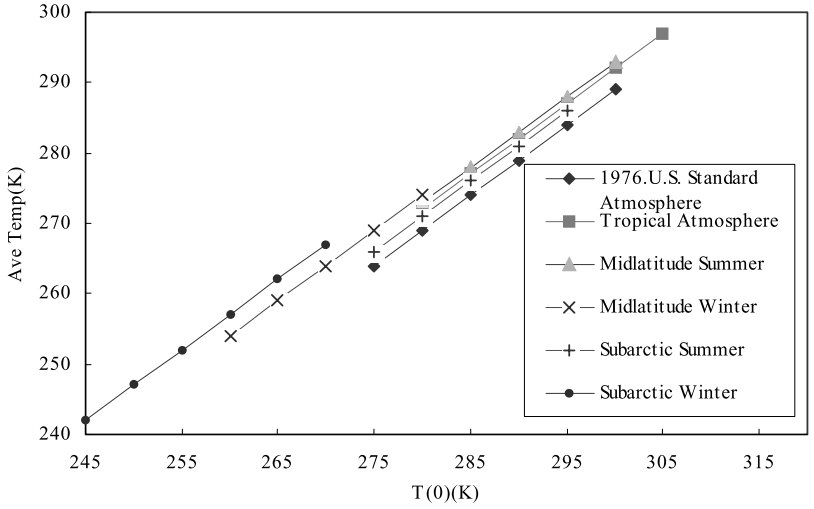

Figure 3. The relationship between effective atmosphere temperature and surface air temperature (in 2 m height).

Table 3. Relationship Between Ta and T_0 for Different Atmosphere Models

Atmosphere Model	Equation	R^2
Tropical atmosphere	$T_a = T_0 - 8.333$	0.997
Midlatitude summer	$T_a = 0.98T_0 - 1.6$	0.9954
Midlatitude winter	$T_a = 0.94T_0 + 9.8$	0.9986
Subarctic summer	$T_a = 1.02T_0 - 14.5$	0.9973
Subarctic winter	$T_a = T_0 - 3$	1
USA.1976	$T_a = T_0 - 11$	1

posed problem can be overcome if more detailed classification can be obtained.

3.2. Connection Between Land Surface Temperature, Brightness Temperature at Satellite, and Average Atmosphere Temperature

[16] The effective average atmosphere temperature (T_a) varies with the wavelength, so we should build different equation for different wavelength in a strict way. In this section, we just analyze the relationship between effective average atmosphere temperature and brightness temperature at satellite, and land surface temperature using the standard atmosphere simulation without considering the influence of wavelength. Atmosphere temperature is changed with surface air temperature (about two meter height) under about 13 km and the profile shape of atmosphere temperature for six standard atmosphere models is like Figure 2.

[17] We change the parameter water vapor content in MODTRAN4 and find the ratio of atmosphere water vapor content in every layer is very stable for every atmosphere model (like Table 2). *Qin et al.* [2001a, 2001b] made a similar analysis by using LOWTRAN7.

[18] From Figure 2 and Table 2, according to expression (6), we compute the effective average atmosphere temperature through changing surface air temperature (in two meter height) and water vapor content in MODTRAN4. The relationship between effective average atmosphere temperature and surface air temperature is like Figure 3.

[19] As shown in Figure 3, the effective average atmosphere temperature has a good linear function with near surface air temperature [*Ulaby et al.*, 1986; *Qin et al.*, 2001a, 2001b]. The common expression can be depicted as (10):

$$T_a = A_1 + B_1 T_0 \tag{10}$$

T_0 is surface air temperature at a two meter height above the ground, A_1 is a constant and B_1 is coefficient. Of course, for different atmosphere model and season, the coefficient of equation (10) is different. We can build a LUT (look up table like Table 3).

[20] The land surface temperature has some difference with the surface air temperature at two meter height above the ground because there is heat exchanging. If we know surface air temperature in two meter height from ground meteorology station, the effective average atmosphere temperature will be estimated. Unfortunately, we cannot obtain so much global ground data in two meter height. The surface air temperature is influenced by land surface temperature, so the difference is not very large in most conditions. We assume -5 k $< T_s - T_0 < 5$ K, and the Figure 4 is the simulated results when the difference is ±5 K for every atmosphere model. Table 4 gives error of effective average atmosphere temperature estimated from LST when the difference is under ±5 K between LST and surface air temperature. The computational method is that we make the land surface temperature (T_s) instead of surface air temperature (T_0). In fact, the ratio of water vapor content near land surface (see equation (6)) is very little. So the error is very small for product of water vapor content ratio in first layer (0 km in Table 2) and the difference between T_s and T_0. As shown in Table 4, the max error of effective average atmosphere temperature estimated from land surface temperarture is not larger than 3 K when difference is under ±5 K between land surface tempeature and surface air tempeature. In fact, the error will be under 1 K if we separate the two meter height from the first layer because the ratio of water vapor content is very small. So the expression can be also depicted as expression (11) when -5 k $< T_s - T_0 < 5$ K.

$$T_a \approx A_2 + B_2 T_s \tag{11}$$

[21] When $|T_s - T_0| > 5$ *K*, the ratio of water vapor content is smaller than 1% (2 m/1000 m) under two meter height if the distribution of water content is assumed as uniform distribution in 1 km range. The error of effective average atmosphere temperature estimated from expression (6) is not very large, but the relationship cannot be depicted as a good linear equation between T_a and T_s, which makes the situation more complex.

[22] On the other hand, if we make the pixel at satellite as an emission object, the effective atmosphere temperature has maybe a better linear relationship with the brightness temperature at satellite according to the reciprocity theory even if we omit the influence of land surface temperature. The expression can be depicted as equation (12).

$$T_a \approx A_3 + B_3 T_i \tag{12}$$

where T_i is the brightness temperature at satellite. The error will be smaller. However, seen from the equations (5), the coefficient (transmittance and emissivity) is smaller than 1. So the error of effective average atmosphere temperature does not influence much (less than 1 K) for land surface temperature retrieval because the coefficient is smaller than 1. To some extent, the land surface temperature, brightness temperature at satellite and average atmosphere temperature are connected with each other. However, the relationship cannot be depicted in embodiment (a strict mathematics equation), the error will be much large sometimes when we resolve the retrieval equations. The at least squares and neural network methods will be the best methods in the geophysical parameter retrieval when the relationship cannot be depicted by using strict mathematics equation.

[23] In a word, there are some linear relationships between effective average atmosphere temperature, land surface temperature and brightness temperature at satellite. In fact, seen from equations equations (5) after linear simplification for Planck function, the linear relationship between effective average atmosphere temperature, land surface temperature, and brightness temperature at satellite is con-

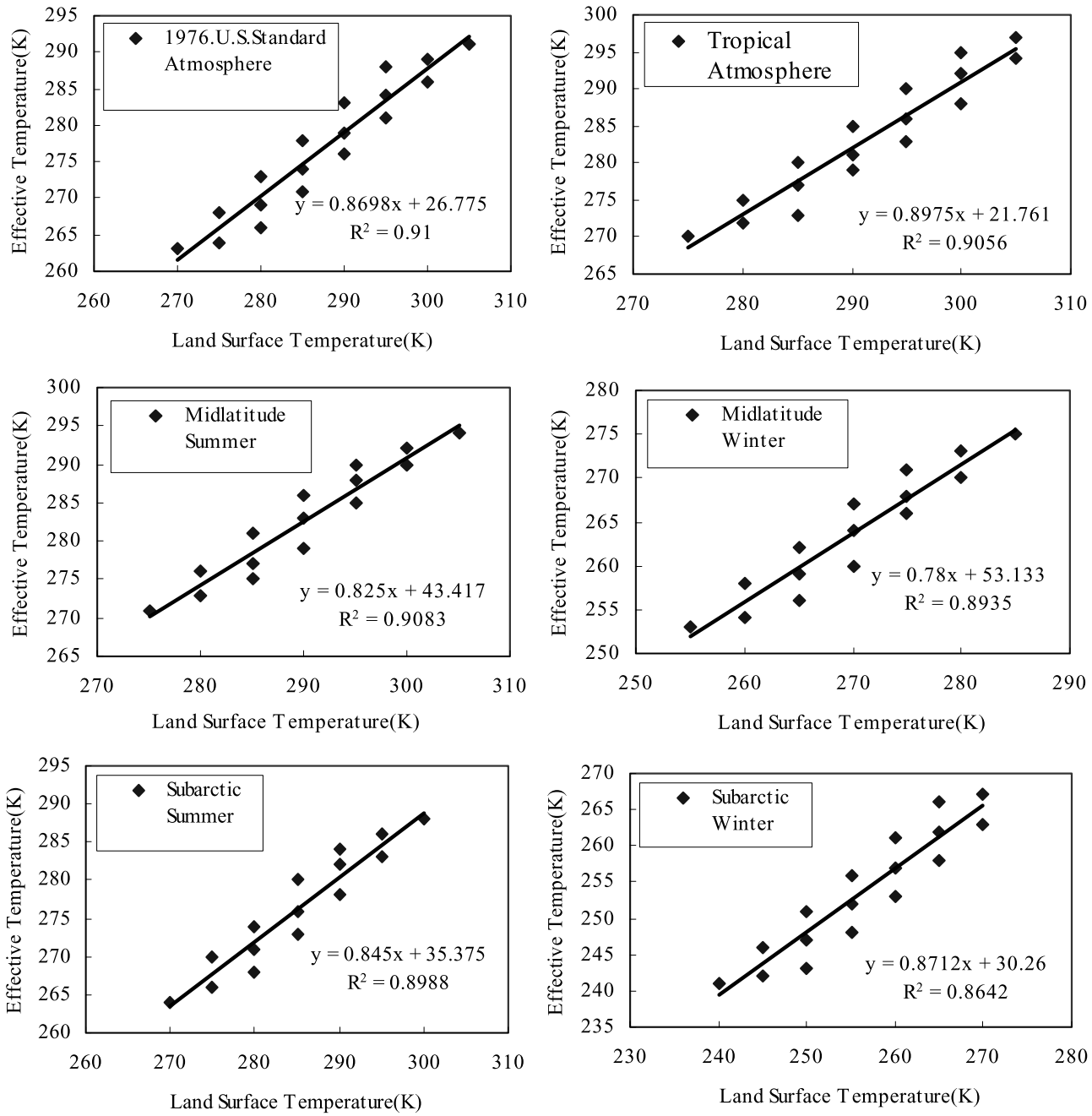

Figure 4. The relationship between effective average atmosphere temperature and land surface temperature when $-5\ \mathrm{k} < T_s - T_0 < 5\ \mathrm{K}$.

trolled by emissivity and transmittance. In thermal band, the transmittance is mainly determined by water vapor content.

3.3. Connection Between Atmospheric Water Vapor Content and Transmittance

[24] The transmittance of atmosphere is a key parameter for land surface temperature retrieval. Transmittance is often got from atmospheric simulation by using atmosphere model (6S, LOWTRAN, MODTRAN, etc.). Because of many technical difficulties, atmospheric transmittance is usually not available in situ when satellite passes. The most practical way to determine the atmospheric transmittance is through simulation with local atmosphere conditions, especially water vapor content. Among the 36 bands of MODIS, five of them are NIR bands (2(0.865 μm), 17(0.905 μm), 18(0.936 μm), 19(0.940 μm), and 5(1.24 μm)). Bands 17, 18, and 19 are three absorption bands, but bands 2 and 5 are atmosphere window bands. The five bands can be used to retrieve the water vapor content of atmosphere from the MODIS image. The retrieval water vapor content algorithm from NIR band can be referred to [*Kaufman and Gao*, 1992; *Sobrino et al.*, 2004; *Mao et al.*, 2005a, 2005b, 2005c].

[25] Because the transmittance of thermal band is mainly influenced by atmosphere water vapor content, we obtain the statistical relationship between the transmittance of MODIS bands 29, 31, and 32, and atmosphere water vapor

Table 4. Error of Effective Atmosphere Temperature Estimated From LST When $-5\ \mathrm{k} < T_s - T_0 < 5\ \mathrm{K}$

$Ts - T(0)$	Error	Tropical	Midlatitude Summer	Midlatitude Winter	Subarctic Summer	Subarctic Winter	USA 1976
±5 K	Ave	2.20	1.85	1.85	2.00	2.60	2.22
±5 K	RMS	2.52	2.14	2.19	2.31	3.00	2.58
±4 K	Ave	1.72	1.65	1.58	1.67	1.98	1.65
±4 K	RMS	1.95	1.89	1.78	1.83	2.29	1.87
±3 K	Ave	1.2	1.26	1.31	1.34	1.36	1.27
±3 K	RMS	1.38	1.45	1.5	1.53	1.57	1.53
±2 K	Ave	1.11	0.95	0.91	0.97	1.03	0.96
±2 K	RMS	1.23	1.08	1.04	1.11	1.29	1.12
±1 K	Ave	0.48	0.61	0.48	0.53	0.68	0.39
±1 K	RMS	0.49	0.7	0.61	0.58	0.81	0.45
±0 K	Ave	0.33	0.4	0.48	0.2	0	0
±0 K	RMS	0.333	0.42	0.58	0.24	0	0

content by simulation of MODTRAN4. Figure 5 is the simulation result.

[26] We make a regression for these data. The expressions can be written as:

$$\text{For band } 29: \tau_{29} = 1.548e^{\frac{w}{-14.489}} - 0.663, \quad R^2 = 0.999 \quad (13a)$$

$$\text{For band } 31: \tau_{31} = 2.9 - 1.88e^{\frac{w}{21.23}}, \quad R^2 = 0.998 \quad (13b)$$

$$\text{For band } 32: \tau_{32} = 4.6e^{\frac{w}{-32.71}} - 3.59, \quad R^2 = 0.997 \quad (13c)$$

[27] From the analysis above, there are three radiance transfer equations, and there is local linear relationship between different band emissivities, and there is some linear relationship (at least control conditions) between effective average atmosphere temperature, land surface temperature, and the brightness temperature at sensor. On the other hand, the transmittance can be determined by water vapor content. Many atmospheric constituents such as carbon dioxide, nitrogen oxide, ozone oxide, methane, carbon monoxide, and other gases have some impacts for transmittance, although which can be assumed as constant and simulated by standard atmospheric profiles. In fact, the relationships are more complicated than the analysis above through the spectral database provided by JPL and simulation data by MODTRAN4. The atmospheric temperature and water vapor profiles vary much wider ranges over land than over ocean [*Wan and Dozier*, 1989]. On the other hand, the effective average atmosphere temperature varies with the wavelength dependence of the water vapor absorption. We cannot assign an effective average atmosphere temperature for different band in a strict manner. However, the coefficient is smaller than 1, so the influence is slight, especially when we use iterative method (such as neural network) to resolve retrieval equations. The development of a general physical algorithmic procedure and a set of rules undertaking that is costly and time consuming, which determines that the neural network is one of the best ways to retrieve land surface temperature and emissivity from MODIS1B data. To some extent, neural network is an optimal algorithm which can make the error of retrieved parameter smallest (see section 4).

4. RM-NN to Solve the Ill-Posed Problem

[28] In section 2 and 3, we show that the land surface temperature and emissivity can be retrieved through three thermal radiance equations and additive equations or conditions (interconnection between geophysical parameters). In this section, we mainly use radiative transfer model (MODTRAN4) and neural network to resolve the ill-posed problem. Many studies have proved the inherent capabilities of the neural network to perform function approximation, classification and optimization [*Hornik et al.*, 1989; *Hsu et al.*, 1992; *Fung*, 1994]. The complicated relationship between geophysical parameters determines that neural network is the one of the best ways to solve the ill-posed problem.

4.1. Why Use Neural Networks

[29] Neural networks, with their remarkable ability to derive meaning from complicated or imprecise data, can be used to extract patterns and detect trends [*Hsu et al.*, 1992]. The neural network (NN) is much different from conventional algorithm requiring that the inversion algorithm be known exactly. For the geophysical parameters retrieval from remote sensing data, this may be quite difficult because of the many nonlinear and poorly understood factors involved. The NN, in contrast to conventional methods, does not require that relationship between the input parameters and the output parameters be known, which determines the relationship between inputs the outputs directly from the training data [*Fung*, 1994].

4.2. Multiple Neural Networks

[30] As shown in Figure 6, multiple neural network (MNT) consists of multiple layers of basic processing units, which are commonly referred to as neurons. The individual

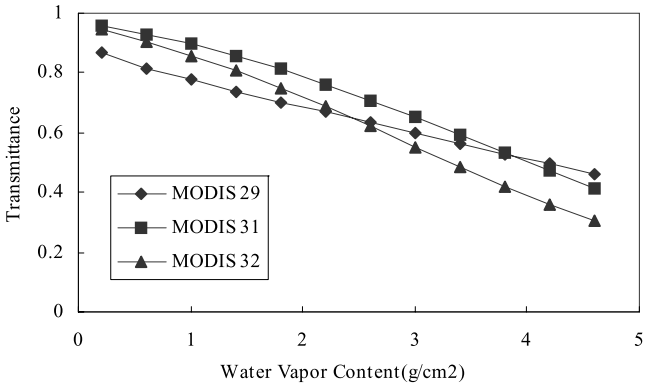

Figure 5. Atmosphere transmittance as function of water vapor content (under midlatitude atmosphere).

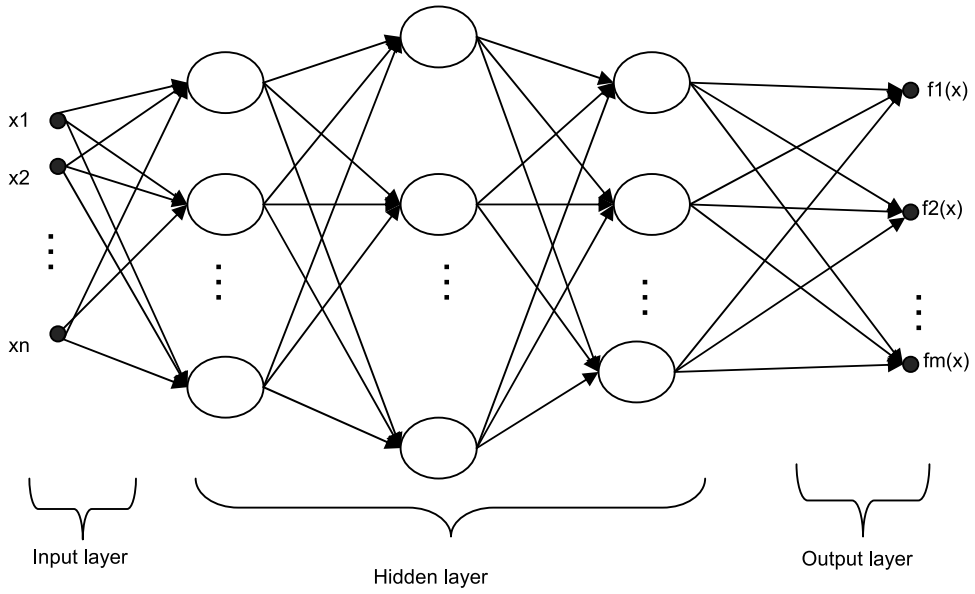

Figure 6. Multiple neural networks.

neuron is the element of each layer within the network. The neuron can be viewed as an element which processes one or more input signal x by (1) taking its inner product with a weight vector w and then adding a bias term σ and (2) putting the resultant number through a generally nonlinear activation function to produce a single output termed the activation level of that neuron.

[31] The sum $x \cdot w + \sigma$ is commonly termed the Net of the neuron. Figure 7 indicates the arrangement of an individual neuron. The input to the neuron can either be the actual input to the system x or the output from other neurons in preceding layers as shown in Figure 6.

[32] The activation function $f(Net)$ has many forms. The most common activation function is the nonlinear sigmoid function given by

$$f(Net) = \frac{1}{1 + e^{-Net}} = \frac{1}{1 + e^{-(w \cdot x + \sigma)}} \tag{14}$$

The representation of the function by the neural network is accomplished by a set of individual neurons that have learned the appropriate response to an input. During the training phase of the supervised network, training patterns are sequentially presented to the network. After all patterns have been presented, the interconnecting synaptic strength (weights) of each neuron are adjusted such that the functional approximation created by the neural network minimizes the global error between the desired output and the summed output created by network given by expression (15)

$$Error = \sum_p E_p = \frac{1}{2} \sum_p \sum_i \left[T_{pi} - a_{pi} \right]^2 \tag{15}$$

where T_{pi} is the ith desired output of the pth training pattern, and a_{pi} is the corresponding activation level of the ith unit in the output layer, in expression above, the values of i are summed only for output units. We can think of the trained

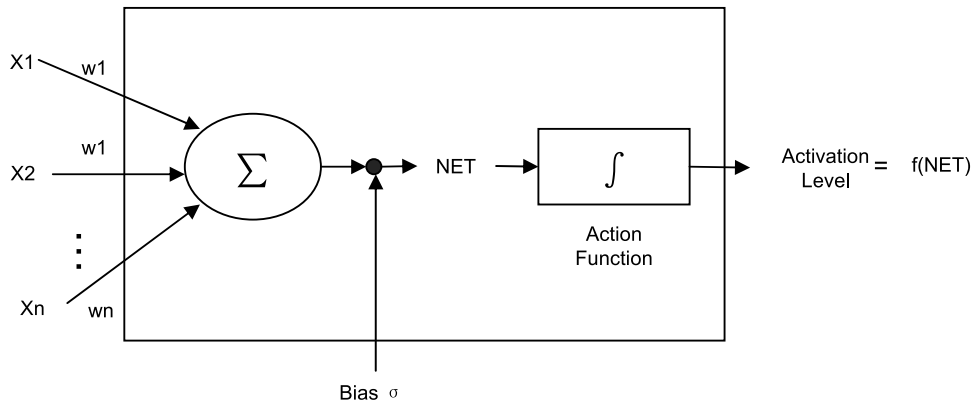

Figure 7. A single neuron.

Table 5. Summary of Retrieval Error[a]

	LST		EM 29		EM 31		EM 32	
Hidden Nodes	R	SD	R	SD	R	SD	R	SD
100–100	0.995	1.63	0.955	0.018	0.922	0.016	0.906	0.02
200–200	0.996	1.5	0.958	0.017	0.938	0.014	0.938	0.015
300–300	0.996	1.45	0.958	0.017	0.942	0.013	0.938	0.015
400–400	0.998	0.95	0.975	0.013	0.968	0.01	0.968	0.01
500–500	0.994	1.77	0.961	0.016	0.951	0.013	0.953	0.013
600–600	0.999	0.55	0.984	0.01	0.978	0.008	0.976	0.009
700–700	1	0.51	0.988	0.009	0.985	0.007	0.986	0.007
800–800	**1**	**0.48**	**0.988**	**0.009**	**0.984**	**0.007**	**0.984**	**0.008**
900–900	1	0.52	0.986	0.01	0.983	0.008	0.983	0.008

[a]R, correlation coefficient; SD, Standard deviation of the fit.

neural network as a type of nonlinear least mean squares interpolation formula for the discrete set of data points in the training set. Clearly, the accuracy of the approximation is dependent on the training data. More introduction is given by *Fung* [1994].

4.3. Training and Testing of RM-NN for Parameter Retrieval

[33] The relationship between geophysical parameters in section 3 has not been used in real retrieval course. The analysis between geophysical parameters just proves the neural network is one of the best methods to retrieve land surface temperature and emissivity. The implementation of RM-NN algorithm is very simple and can be broken into four basic steps: (1) simulating the training and testing data by MODTRAN4, or obtaining the reliable field measurement data, including the high accuracy of MODIS LST and emissivity product in reliable research region, (2) training and testing neural network, (3) computing the brightness temperature of bands 29, 31, and 32, and retrieving water vapor content from MODIS bands 2, 5, 17, 18, 19, or other sensor, and (4) retrieving land surface temperature and emissivity by using neural network.

[34] Seen from the analysis in section 2 and 3, the retrieval equations are fewer than unknowns. However, the relationships between geophysical parameters are many. The relationship of emissivity between MODIS bands 29/31/32 (8∼13.4 μm) can be kept well through radiance transfer model (MODTRAN4) simulation, which is very difficult to keep in field measurement. In this section, we use MODTRAN4 to simulate the radiance transfer course of MODIS bands 29/31/32 and the water vapor content retrieved from VIR-NIR band as the training and testing data which can be viewed as reference data from a known ground truth. These emissivities (like Figure 1) of bands 29/31/32 are made as input parameters in MODTRAN4. The range of land surface temperature is from 270 to 320 K, and the corresponding surface air temperature (at 2 m height) is arbitrarily assumed from 273 to 310 K. The range of atmosphere water vapor content is from 0.2 to 4.5 g cm^2. We divide randomly the simulation data into two parts: training data with 7760 set and testing data with 634 set. Then, we use dynamic learning neural network (DL) [*Tzeng et al.*, 1994] to solve ill-posed retrieval problem. First, we use training data to train the neural network, and then use testing data to verify the neural network. According to the number of surface types and trial and error, the detail test data sets information can be referred as in Table 5.

[35] As shown in Table 5, the accuracy is the highest when the number of hidden layer is two and the number of hidden node is 800–800, which is mainly determined by the number of surface types, the simplification of Planck function, and the relationship between water vapor content and transmittance. We make a comparison between retrieval

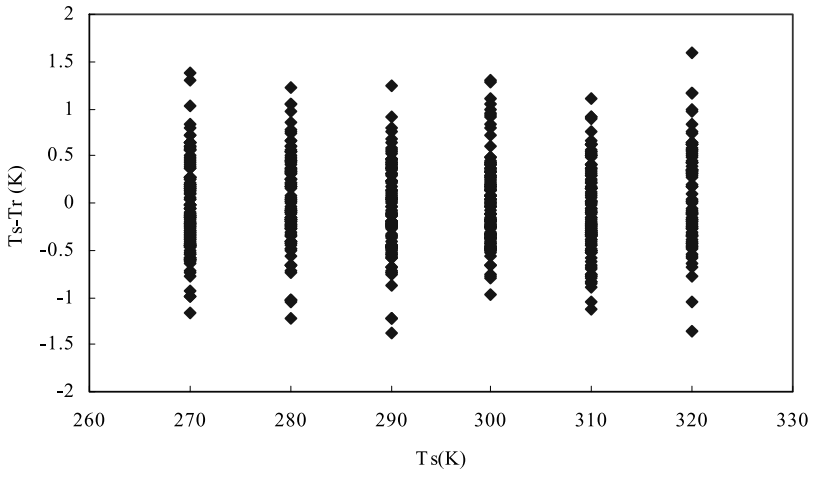

Figure 8a. The difference distribution between truth land surface temperature and retrieval land surface temperature.

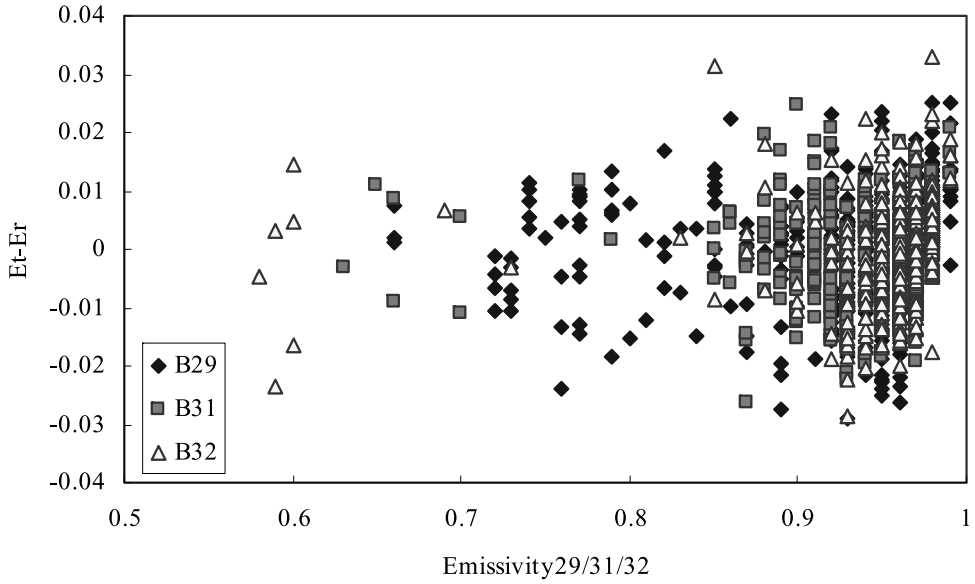

Figure 8b. The difference distribution between truth land surface emissivity and retrieval land surface emissivity.

land surface temperature/emissivity and truth land surface temperature/emissivity for test data. As shown in Figures 8a and 8b, the retrieval result is very good and the error is very small. The average error ($\frac{\sum_{i}^{n} |T_s - T_r|}{n}$) of land surface temperature is under 0.4°C. The average error of emissivity in band 29 is under 0.008. The average error of emissivity in band 31 and is under 0.006.

4.4. Sensitivity Analysis of Parameter Water Vapor Content

[36] The atmosphere water vapor content is an important input parameter, which determines the transmittance in radiance transfer equation. A sensitivity analysis for water vapor content is necessary because the influence of atmosphere water vapor content for thermal radiance transfer is large. The most retrieval error of water vapor content from NIR (MODIS2/5/17/18/19) is from −13% to +13% in clear day [*Kaufman and Gao*, 1992], so we make an retrieval error analysis for neural network when retrieval error of water vapor content is between −15% and +15%. The result is listed in Table 6.

[37] As shown in Table 6, neural network is not sensitivity when the retrieval error is between −13% and +13%. On the other hand, we can make the network more robust through making some error for parameter water vapor content in training data.

5. Comparison With MODIS LST Product and Evaluation

[38] In order to give an application example, we use this DL neural network, which has been trained to retrieve the land surface temperature and emissivity from MODIS1B data. The inputs of neural network are brightness temperature (T_i, i = 29/31/32) and the water vapor content retrieved from MODIS bands 2/5/17/18/19, and the outputs are the land surface temperature and emissivity. We select the MODIS/TERRA image of Shandong peninsula, China,

Table 6. Sensitivity Analysis of Water Vapor Content

Water Vapor Content Error	LST		EM 29		EM 31		EM 32	
	R	SD	R	SD	R	SD	R	SD
15%	0.997	1.23	0.941	0.019	0.93	0.015	0.917	0.017
13%	0.998	1.05	0.958	0.016	0.949	0.013	0.938	0.015
10%	0.999	0.85	0.973	0.013	0.966	0.01	0.96	0.012
7%	0.999	0.69	0.98	0.011	0.976	0.009	0.974	0.01
5%	0.999	0.61	0.983	0.01	0.98	0.008	0.979	0.009
2%	0.999	0.53	0.986	0.01	0.983	0.008	0.983	0.008
0%	1	0.48	0.988	0.009	0.984	0.007	0.984	0.008
−2%	1	0.51	0.986	0.009	0.983	0.008	0.983	0.008
−5%	0.999	0.586	0.984	0.01	0.982	0.008	0.98	0.009
−7%	0.999	0.664	0.982	0.01	0.98	0.008	0.977	0.009
−10%	0.998	0.81	0.977	0.012	0.977	0.009	0.972	0.01
−13%	0.998	0.97	0.97	0.014	0.973	0.01	0.967	0.011
−15%	0.998	1.09	0.965	0.015	0.97	0.01	0.963	0.012

R: Correlation coefficient; SD: Standard deviation of the fit.

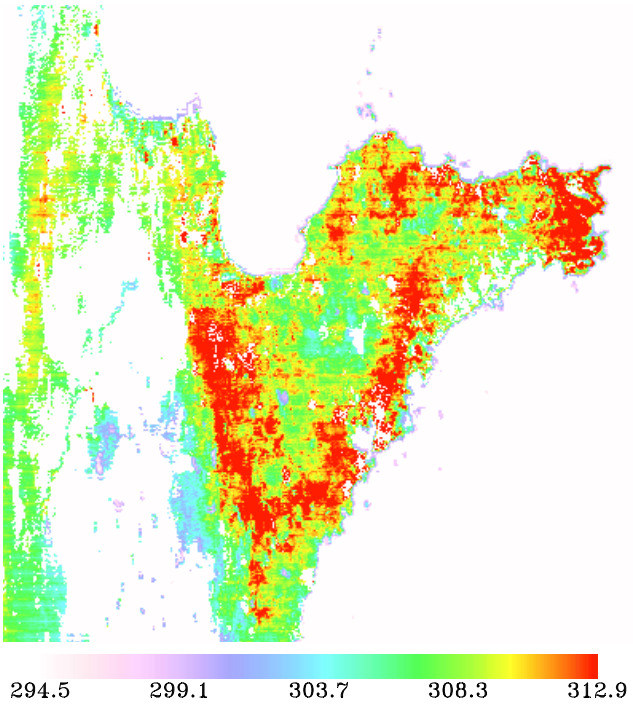

Figure 9a. Retrieval by RM-NN.

9 September 2005 as the research region and make retrieval results compare with MODIS product. Figure 9a is the retrieval result by RM-NN, which has stripes because of the influence of band 29. Figure 9b is MOD11_L2 LST_1KM Product. The product of MOD11_L2 LST_1KM is MODIS/TERRA land surface temperature/ emissivity 5-MIN L2 swath 1 V004, which provides per pixel temperature and emissivity values. Temperatures are

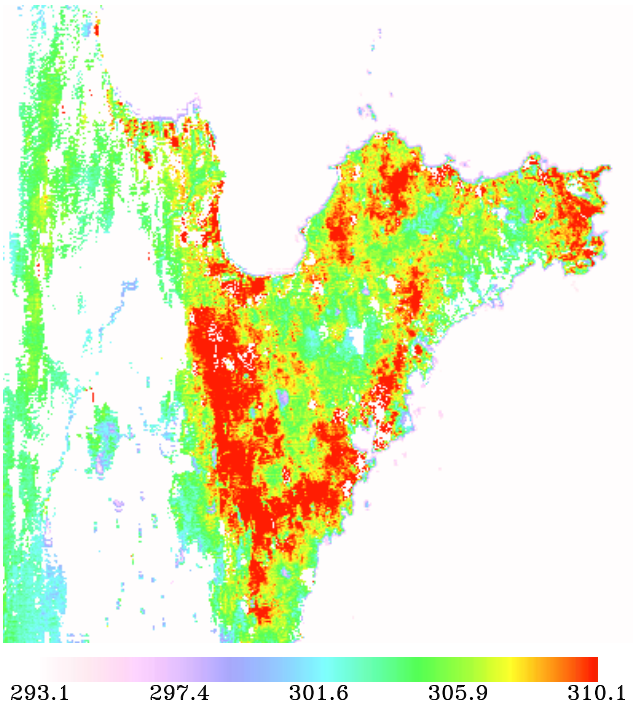

Figure 9b. MOD11_L2 LST_1KM product.

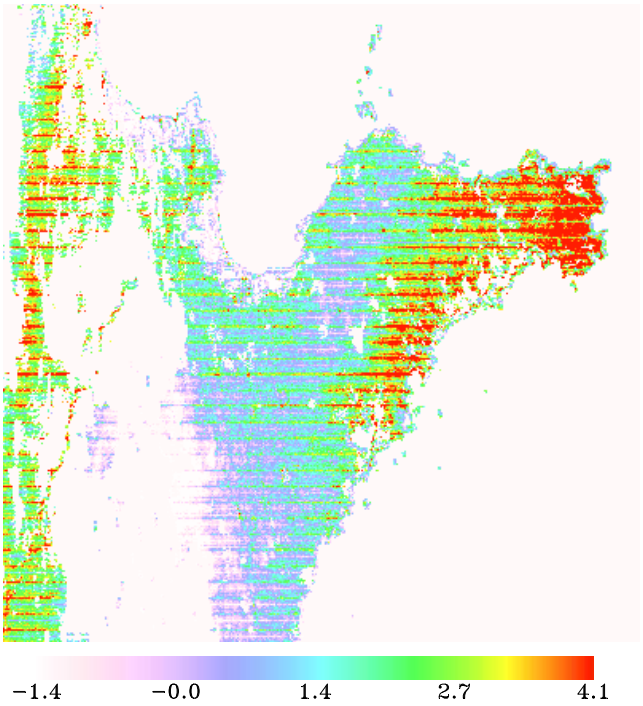

Figure 10a. The difference between Figures 9a and 9b (land surface temperature).

extracted in Kelvin with the generalized split window LST [*Wan*, 1999; *Wan and Dozier*, 1996]. Emissivities are derived from land cover database information. Figure 10a is the difference distribution of land surface temperature between result by RM-NN and MOD11_L2 LST_1KM Product, and Figure 10b is the histogram of the Figure 10a. As shown in Figures 10a and 10b, most retrieval result by RM-NN is higher than MODIS LST product.

[39] In MODIS product (matching to Figure 9b), most emissivity values are 0.986 in band 31 for all pixels, and most values are 0.99 for almost all pixels except a few are 0.986 or 0.988 for band 32. The land surface temperature retrieved by RM-NN is higher than MODIS LST product (the range is from -1.4°C to 4.1°C) and the average difference is about 1.3°C. Figures 11a–11c show the difference of emissivity between MODIS product and retrieval result by RM-NN. The distribution of Figures 11a and 11b is similar with Figure 10a. Figure 11c is the histogram of relative error of emissivity in Figures 11a and 11b. Most of emissivity in bands 31 and 32 retrieved by RM is lower than MODIS product.

[40] The retrieval results are reasonable and the reason is that MOD11_L2 LST_1KM product overestimates the emissivity, which makes MODIS product LST is lower than land surface temperature retrieved by RM-NN. The generalized split-window LST algorithm [*Wan*, 1999; *Wan and Dozier*, 1996] yields 1 K accuracy for materials under the condition of known emissivities. To some extent, the error of estimated emissivity will influence land surface temperature retrieval error in this algorithm. It is not very reasonable that the emissivity is almost same in product (matching to Figure 9b), which also indicates the limitation of the split window algorithm.

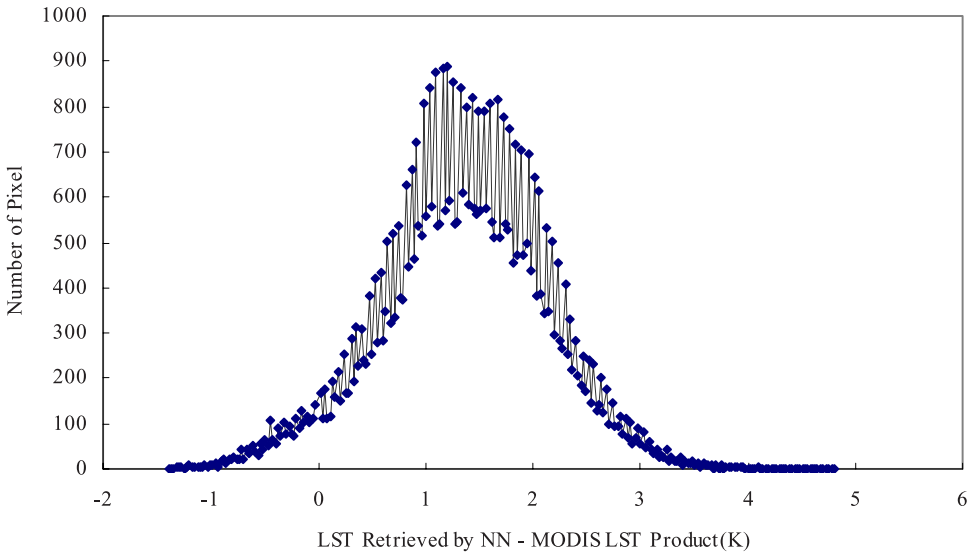

Figure 10b. The histogram of Figure 10a (land surface temperature).

[41] On the other hand, we made an analysis with the product MOD11B1 (MODIS_Grid_Daily_5km_LST) (like Figure 12), which retrieved by day/night LST algorithm [*Wan*, 1999]. The range of emissivity in band 31 is from 0.922 to 0.996 and the range of emissivity in band 32 is from 0.916 to 0.996. This product also indicates that the emissivity retrieved by the generalized split window algorithm [*Wan*, 1999; *Wan and Dozier*, 1996] overestimates the emissivity and underestimates the land surface temperature. The matching is a problem because of project and the resolution (1 km by RM-NN, 5 km by day/night LST algorithm), so we do not compare results retrieved by RM-NN with day/night LST algorithm from pixel to pixel. The statistical analysis indicates that the retrieval results of RM-NN are lying between the two products provided by NASA, and very close to the day/night LST algorithm. We make a regression revision and the average error is 0.36°C relative to MODIS LST product(MOD11_L2) retrieved by

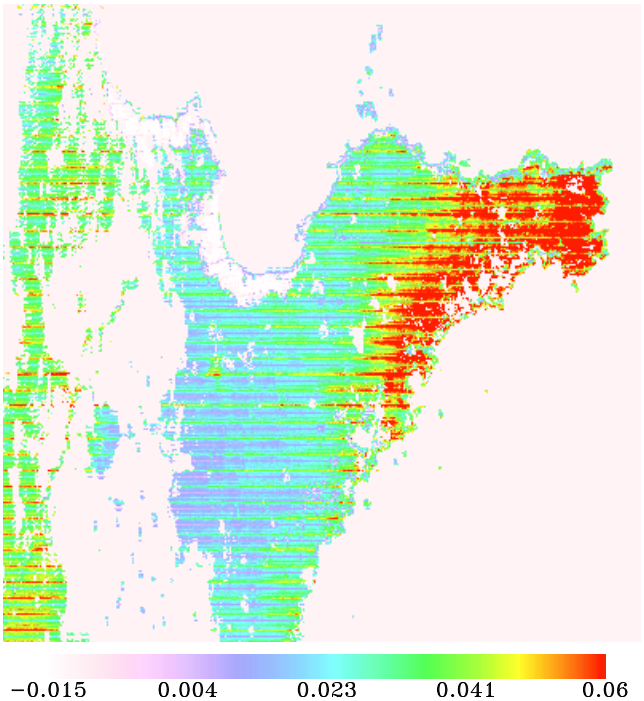

Figure 11a. The difference in band 31 between MODIS product emissivity and retrieval by RM-NN (MODIS product−RM-NN).

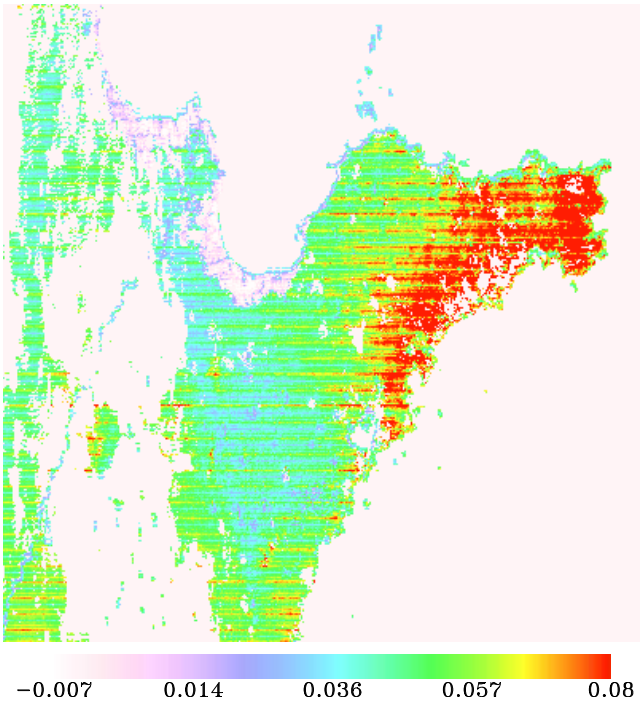

Figure 11b. The difference in band 32 between MODIS product emissivity and retrieval by RM-NN (MODIS product−RM-NN).

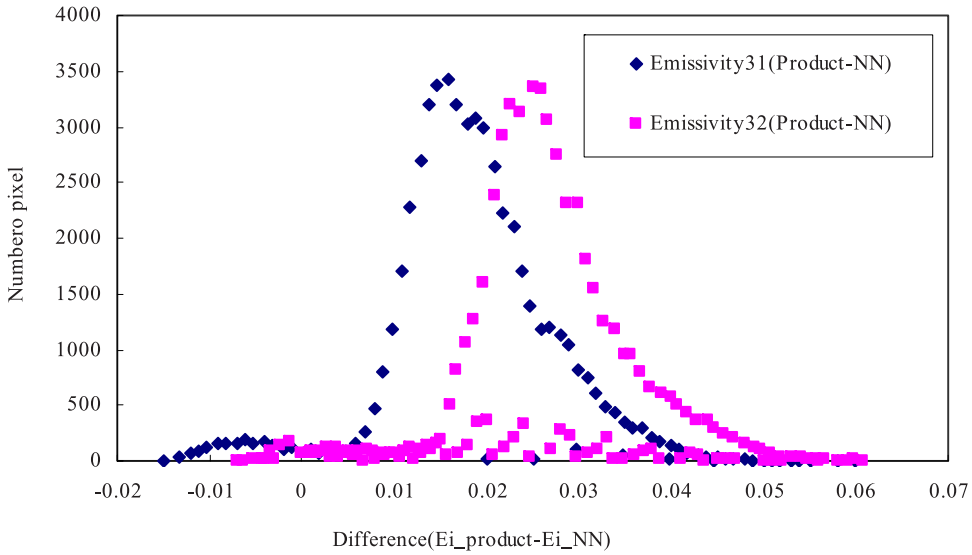

Figure 11c. The histogram of Figures 11a and 11b.

generalized split window LST algorithm [*Wan*, 1999; *Wan and Dozier*, 1996]. In this study, we mainly want to prove that RM-NN is available to retrieve accurately land surface temperature and emissivity simultaneously.

[42] It is very difficult to obtain the in situ ground measurement of LST matching at the pixel scale (1 km * 1 km at nadir) to MODIS data at the satellite pass for the validation of algorithm. Generally speaking, LST varies from point to point on the ground, and ground measurement is generally point measurement. It is a problem to obtain the measured LST matching the pixel of MODIS data. On the other hand, MODIS observes the ground at different angles, and precisely locating the pixel of the measured ground in MODIS data (especially night images) is also a problem. In addition to these difficulties, ground emissivity and the in situ atmospheric conditions also have to be known for the validation. Since there are so many difficulties in obtaining ground truth data, validation with the use of ground truth data is quite difficult. The project 973 of China made ground experiments in Xiaotangshan and provided a data set of two sites (116.448E and 40.182N, 116.447E, and 40.177N). *Han* [2006] estimated the land surface temperature and compared with MOD11_L2 LST_1KM product, which indicated that MODIS 1 km product underestimates the land surface temperature. We extract the MODIS pixels from MODIS 1B data by using a program through the longitude/latitude conditions. The comparison between result by RM-NN and ground land surface is shown in Figure 13 and the average accuracy is about 1.03 K. As we all know, there are many influence factors for ground land surface temperature measurement, especially for mixed pixel. *Wang and Liang* [2005] made much analysis by comparing MODIS LST product and FLUXNET database (http://public.ornl.gov/ameriflux/datahandler.cfm), which indicated that constant emissivity values used by MODIS split window algorithm may need to be adjusted. We will make more field measurement, and more comparison analysis will be reported in the future. On the other hand, another advantage of the RM-NN is that the retrieval accuracy can be improved and suitable for more conditions by compensating more training data including high-accuracy MODIS LST product.

6. Conclusion

[43] The ill-posed problem of land surface temperature and emissivity retrieved from MODIS data is discussed. The relationships are explored between different band emissivities in MODIS bands 29, 31, and 32, between land surface temperature, brightness temperature at satellite, and effective average atmosphere temperature, and also between transmittance and water vapor content. The analysis indicates that the radiance transfer model (RM)–neural network (NN) can be competent for resolving these ill-posed prob-

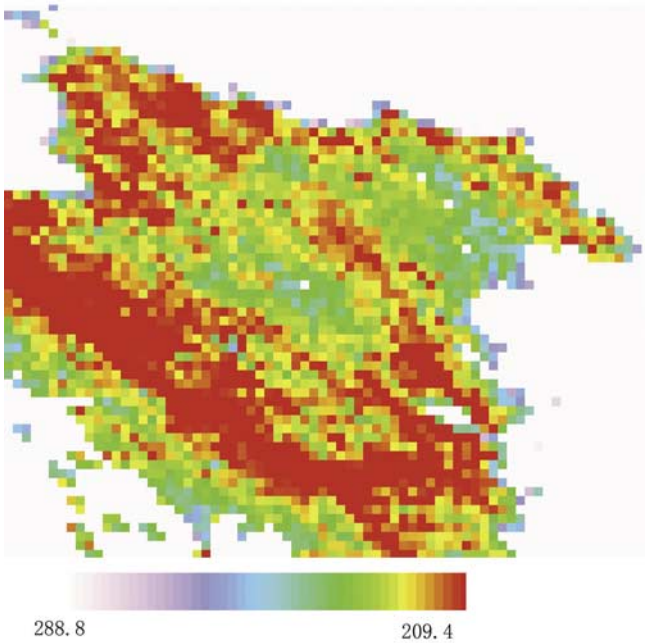

Figure 12. MOD11B1_5KM product.

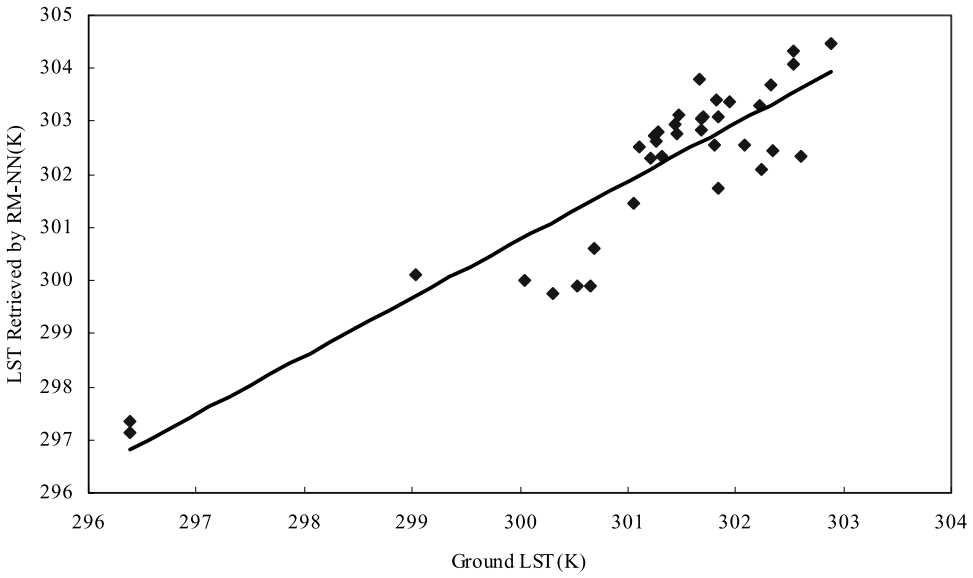

Figure 13. Validation results by *Han* [2006].

lems (LST and emissivity retrieval), because the geophysical parameters have some interconnections, which cannot be depicted by using strict mathematics equations.

[44] We utilize the MODTRAN4 to simulate data to train and test neural network. The test results indicate that RM-NN is very robust. The accuracy is highest when the number of hidden layer is two, and the number of hidden node is 800–800. Simulation data analysis indicates that the average error of land surface temperature is under 0.4°C, and the average error of emissivity is under 0.008, 0.006, and 0.006 for bands 29, 31, and 32, respectively. We use the trained neural network (DL) to retrieve the land surface temperature and emissivity from MODIS1B for Shandong peninsula. The comparison analysis between result by RM-NN and MODIS product algorithm indicates that the generalized split window LST overestimates the emissivity and underestimates land surface temperature about 1 K. The comparison between retrieval result by RM-NN and ground measurement data in Xiaotangshan also show similar conclusion. The results by RM-NN are more close to day/night LST algorithm after statistics analysis. The average error is 0.36°C relative to MODIS LST product (MOD11_L2) retrieved by generalized split window LST algorithm if we make a regression revision. The main purpose of this study is that we proved that the RM-NN is competent for retrieving land surface temperature and emissivity simultaneously. Our algorithm overcomes the difficulty that a single multispectral thermal measurement with N bands presents N equations with N + 1 unknowns (N spectral emissivities and LST).

[45] The ease to implement the RM-NN technique can be implemented and the quality of its results makes it a powerful tool, whose advantages has not been fully utilized by thermal remote sensing. The using RM-NN to perform inversion is an important advancement in thermal remote sensing field and makes it possible to perform inversion with higher accuracy and more practical. We will make some field measurements, and more comparison analysis will be reported in future, to make the RM-NN suitable for more conditions and robust.

[46] **Acknowledgments.** The author would like to thank the following people for their various help with this study: Zhengming Wan, University of California, Santa Barbara, USA; Kunshan Chen, Yuchang Tzeng, and Hung Wei Lee, The Center for Space and Remote Sensing Research, National Central University, 32054 Chung-Li, Taiwan, China; Shunlin Liang, Department of Geography, University of Maryland, College Park, USA; Zhihao Qin and Manchun Li, Nanjing University, China; and JPL for providing the ASTER Spectral Library data and NASA for providing MODIS data. They would also like to thank the anonymous reviewers for their valuable comments, which greatly improved the presentation of this paper. This work was sponsored by the National Natural Science Foundation of China (grant 40571101), basic research work of Central Scientific Research Institution for Public Welfare, Key Laboratory of Resources Remote Sensing and Digital Agriculture, MOA, and Open Fund of Laboratory for Remote Sensing Science, Institute of Remote Sensing Applications of Chinese Academy of Sciences, and Beijing Normal University. The State Key Laboratory of Remote Sensing Science is jointly sponsored by the Institute of Remote Sensing Applications of the Chinese Academy of Sciences and Beijing Normal University.

References

Becker, F., and Z. L. Li (1990), Towards a local split window method over land surface, *Int. J. Remote Sens.*, *11*, 369–393.

Berk, A., G. Anderson, P. Acharya, M. Hoke, J. Chetwynd, L. Bernstein, E. Shettle, M. Matthew, and S. Adler-Golden (2003), *MODTRAN4 Version 3 Revision 1 User's Manual*, Air Force Res. Lab., Hanscom Air Force Base, Mass.

Coll, C., V. Caselles, A. Sobrino, and E. Valor (1994), On the atmospheric dependence of the split-window equation for land surface temperature, *Int. J. Remote Sens. Environ.*, *27*, 105–122.

Coll, C., V. Caselles, J. M. Galve, E. Valor, R. Niclòs, J. M. Sánchez, and R. Rivas (2005), Ground measurements for the validation of land surface temperatures derived from AATSR and MODIS data, *Remote Sens. Environ.*, *97*, 288–300.

Dozier, J., and T. H. Painter (2004), Multispectral and hyperspectral remote sensing of alpine snow properties, *Annu. Rev. Earth Planet. Sci.*, *32*, 465–494.

Dozier, J., and S. G. Warren (1982), Effect of viewing angle on the infrared brightness temperature of snow, *Water Resour. Res.*, *18*, 1424–1434.

França, G. B., and A. P. Cracknell (1994), Retrieval of land and sea surface temperature using NOAA-11 AVHRR data in northeastern Brazil, *Int. J. Remote Sens.*, *15*, 1695–1712.

Fung, A. K. (1994), *Microwave Scattering and Emission Models and Their Application*, Artech House, Boston, Mass.

Gillespie, A., S. I. Rokugawa, T. Matsunaga, J. S. Cothern, S. Hook, and A. Kahle (1998), A temperature and emissivity separation algorithm for

Advanced Spaceborne Thermal Emission and Reflection Radiometer (ASTER) images, *IEEE Trans. Geosci. Remote Sens.*, *36*, 1113–1126.

Han, L. J. (2006), Estimation of evapotranspiration by assimilating MODIS LST product into the CLM (in Chinese), Ph.D. diss., Beijing Normal Univ., Beijing, China.

Hook, S. J., A. R. Gabell, A. A. Green, and P. S. Kealy (1992), A comparison of techniques for extracting emissivity information from thermal infrared data for geologic studies, *Remote Sens. Environ.*, *42*, 123–135.

Hornik, K. M., M. Stinchcombe, and H. White (1989), Multilayer feedforward networks are universal approximators, *Neural Networks*, *4*, 359–366.

Hsu, S., T. Masters, M. Olson, M. Tenorio, and T. Grogan (1992), Comparavtive analysis of five neural networks models, *Remote Sens. Rev.*, *6*, 319–329.

Kahle, A. B., and R. E. Alley (1992), Separation of temperature and emittance in remotely sensed radiance measurements, *Remote Sens. Environ.*, *42*, 1–20.

Kaufman, Y. J., and B. C. Gao (1992), Remote sensing of water vapor in the near IR from EOS/MODIS, *IEEE Trans. Geosci. Remote Sens.*, *27*, 145–153.

Kealy, P. S., and S. Hook (1993), Separating temperature and emissivity in thermal infrared multispectral scanner data: Implication for recovering land surface temperatures, *Trans. Geosci. Remote Sens.*, *31*, 1155–1164.

Kerr, Y. H., J. P. Lagouarde, and J. Imbernon (1992), Accurate land surface temperature retrieval from AVHRR data with use of an improved split window algorithm, *Remote Sens. Environ.*, *41*, 197–209.

King, M. D., Y. J. Kaufman, W. P. Menzel, and D. Tanré (1992), Remote sensing of cloud, aerosol, and water properties from the moderate resolution imaging spectrometer (MODIS), *IEEE Trans. Geosci. Remote Sens.*, *30*, 2–27.

Li, Z. L., and F. Becker (1993), Feasibility of land surface temperature and emissivity determination from AVHRR data, *Remote Sens. Environ.*, *43*, 67–85.

Liang, S. (2001), An optimization algorithm for separating land surface temperature and emissivity from multispectral thermal infrared imagery, *IEEE Trans. Geosci. Remote Sens.*, *39*, 264–274.

Mao, K., Z. Qin, J. Shi, and P. Gong (2005a), A practical split-window algorithm for retrieving land surface temperature from MODIS data, *Int. J. Remote Sens.*, *15*, 3181–3204.

Mao, K., J. Shi, Z. Qin, P. Gong, W. Liu, and L. Xu (2005b), A multiple-band algorithm for retrieving land-surface temperature and emissivity from MODIS data, in *IEEE International Geoscience and Remote Sensing Symposium 2005*, vol. 5, edited by S. Liang et al., pp. 3269–3272, Inst. of Electr. and Electr. Eng., Piscataway, N. J.

Mao, K., J. Shi, Z. Qin, and P. Gong (2005c), An advanced and optimized split-window algorithm for retrieving land-surface temperature from ASTER data, paper presented at Ninth International Symposium on Physical Measurements and Signatures in Remote Sensing, Inst. of Geogr. Sci. and Nat. Resour. Res., Beijing, China.

Mao, K., J. Shi, Z. L. Li, Z. Qin, X. F. Wang, and L. M. Jiang (2006), A multiple-band algorithm for separating land surface emissivity and temperature from ASTER imagery, in *IEEE International Geoscience and Remote Sensing Symposium 2005*, vol. III, edited by V. Chandrasekar et al., pp. 1358–1361, Inst. of Electr. and Electr. Eng., Piscataway, N. J.

Otlle, C., and M. Stoll (1993), Effect of atmospheric absorption and surface emissivity on the determination of land temperature from infrared satellite data, *Int. J. Remote Sens.*, *14*, 2025–2037.

Prata, A. J. (1994), Land surface temperatures derived from the advanced very high resolution radiometer and the along-track scanning radiometer: 2. Experimental results and validation of AVHRR algorithms, *J. Geophys. Res.*, *99*, 13,025–13,058.

Price, J. C. (1984), Land surface temperature measurements from the split-window channels of the NOAA-7 AVHRR, *J. Geophys. Res.*, *79*, 5039–5044.

Qin, Z., A. Karnieli, and P. Berliner (2001a), A mono-window algorithm for retrieving land surface tempeature from landsat TM data and its application to the Israel-Egypt border region, *Int. J. Remote Sens.*, *22*, 3719–3746.

Qin, Z., G. Dall' Olmo, A. Karnieli, and P. Berliner (2001b), Derivation of split window algorithm and its sensitivity analysis for retrieving land surface temperature from NOAA-advanced very high resolution radiometer data, *J. Geophys. Res.*, *106*, 22,655–22,670.

Salomonson, V., W. Barnes, P. Maymon, H. Montgomery, and H. Ostrow (1989), MODIS: Advanced facility instrument for studies of the Earth as a system, *IEEE Trans. Geosci. Remote Sens.*, *27*, 145–153.

Schmugge, T., S. J. Hook, and C. Coll (1998), Recovering surface temperature and emissivity from thermal infrared multispectral data, *Remote Sens. Environ.*, *65*, 121–131.

Schmugge, T., A. French, J. C. Ritchie, A. Rango, and H. Pelgrum (2002), Temperature and emissivity separation from multispectral thermal infrared observations, *Remote Sens. Environ.*, *79*, 189–198.

Sobrino, J. A., and V. Caselles (1991), A methodology for obtaining the crop temperature from NOAA-9 AVHRR data, *Int. J. Remote Sens.*, *I2*, 2461–2475.

Sobrino, J. A., Z. L. Li, M. P. Stoll, and F. Becker (1994), Improvements in the split window technique for land surface temperature determination, *IEEE Trans. Geosci. Remote Sens.*, *32*, 243–253.

Sobrino, J. A., J. E. Kharraz, and Z. L. Li (2004), Surface temperature and water vapour retrieval from MODIS data, *Int. J. Remote Sens.*, *24*, 5161–5182.

Tzeng, Y. C., K. S. Chen, W. L. Kao, and A. K. Fung (1994), A dynamic learning neural network for remote sensing applications, *IEEE Trans. Geosci. Remote Sens.*, *32*, 1096–1102.

Ulaby, F. T., R. K. Moore, and A. K. Fung (1986), *Microwave Remote Sensing: Active and Passive*, vol. 1, Artech House, Dedham, Mass.

Vidal, A. (1991), Atmosphere and emissivity correction of land surface temperature measured from satellite data, *Int. J. Remote Sens.*, *12*, 2449–2460.

Wan, Z. (1999), MODIS land-surface temperature algorithm theoretical basis document, version 3.3, *Rep. LST ATBD*, Inst. for Comput. Earth Syst. Sci., Univ. of Calif., Santa Barbara.

Wan, Z., and J. Dozier (1989), Land surface temperature measurement from space: Physical principles and inverse modeling, *IEEE Trans. Geosci. Remote Sens.*, *27*, 268–278.

Wan, Z., and J. Dozier (1996), A generalized split-window algorithm for retrieving land surface temperature measurement from space, *IEEE Trans. Geosci. Remote Sens.*, *34*, 892–905.

Wan, Z., and Z. L. Li (1997), A physics-based algorithm for retrieving land-surface emissivity and temperature from EOS/MODIS data, *IEEE Trans. Geosci. Remote Sens.*, *35*, 980–996.

Wan, Z., Y. Zhang, Y. Q. Zhang, and Z. L. Li (2002), Validation of the land-surface temperature products retrieved from Moderate Resolution Imaging Spectroradiometer data, *Remote Sens. Environ.*, *83*, 163–180.

Wan, Z., Y. Zhang, Y. Q. Zhang, and Z.-L. Li (2004), Quality assessment and validation of the global land surface temperature, *Int. J. Remote Sens.*, *25*, 261–274.

Wang, W., and S. Liang (2005), Validating MODIS land surface temperature product, paper presented at Ninth International Symposium on Physical Measurements and Signatures in Remote Sensing, Inst. of Geogr. Sci. and Nat. Resour. Res., Beijing, China.

Watson, K. (1992), Spectral ratio method for measuring emissivity, *Remote Sens. Environ.*, *42*, 113–116.

Z.-L. Li, Institute of Geographic Sciences and Natural Resources Research, Chinese Academy of Sciences, Beijing 100101, China.

K. Mao and H. Tang, Laboratory of Resources Remote Sensing and Digital Agriculture, Ministry of Agriculture, Hulumber Grassland Ecosystem Observation and Research Station, Institute of Agricultural Resources and Regional Planning, Ministry of Agriculture, Chinese Academy of Agricultural Sciences, Beijing 100081, China. (kebiaomao2004@hotmail.com)

J. Shi, Institute for Computational Earth System Science, University of California, Santa Barbara, Santa Barbara, CA 93106, USA.